Figure S1. Cisplatin exposure induces the accumulation of total ROS and mitochondrial ROS in WT and MDR HCT-116 cells leading to apoptosis in WT cells. WT and MDR HCT-116 cells were treated with 50 μM cisplatin or vehicle for 12 h. (A) Morphological features were analyzed, showing cell membrane blebbing after a cisplatin treatment in WT cells (x200 magnification). (B) The cells were stained with DCFH-DA dye and analyzed by fluorescence microscopy (x200 magnification); fluorescence intensity was measured using the ImageJ software (n=400 cells); one-way ANOVA was used for statistical analysis. (C) The cells were stained with MitoSox dye to determine the mitochondrial ROS levels by fluorescence microscopy (x400 magnification), and (D) the fluorescence intensity was measured using the ImageJ software (n=400 cells); one-way ANOVA was used for statistical analysis. Representative images of apoptosis analysis by flow cytometry in (E) WT and (F) MDR cells. *P<0.05; **P<0.01; ***P<0.001; ****P<0.0001. Cis, cisplatin; DCFH-DA, dichloro-dihydrofluorescein diacetate; FL1 INT, fluorescent light 1-integral time-of-flight; MDR, multidrug resistant; ns, not significant; ROS, reactive oxygen species; WT, wild-type.

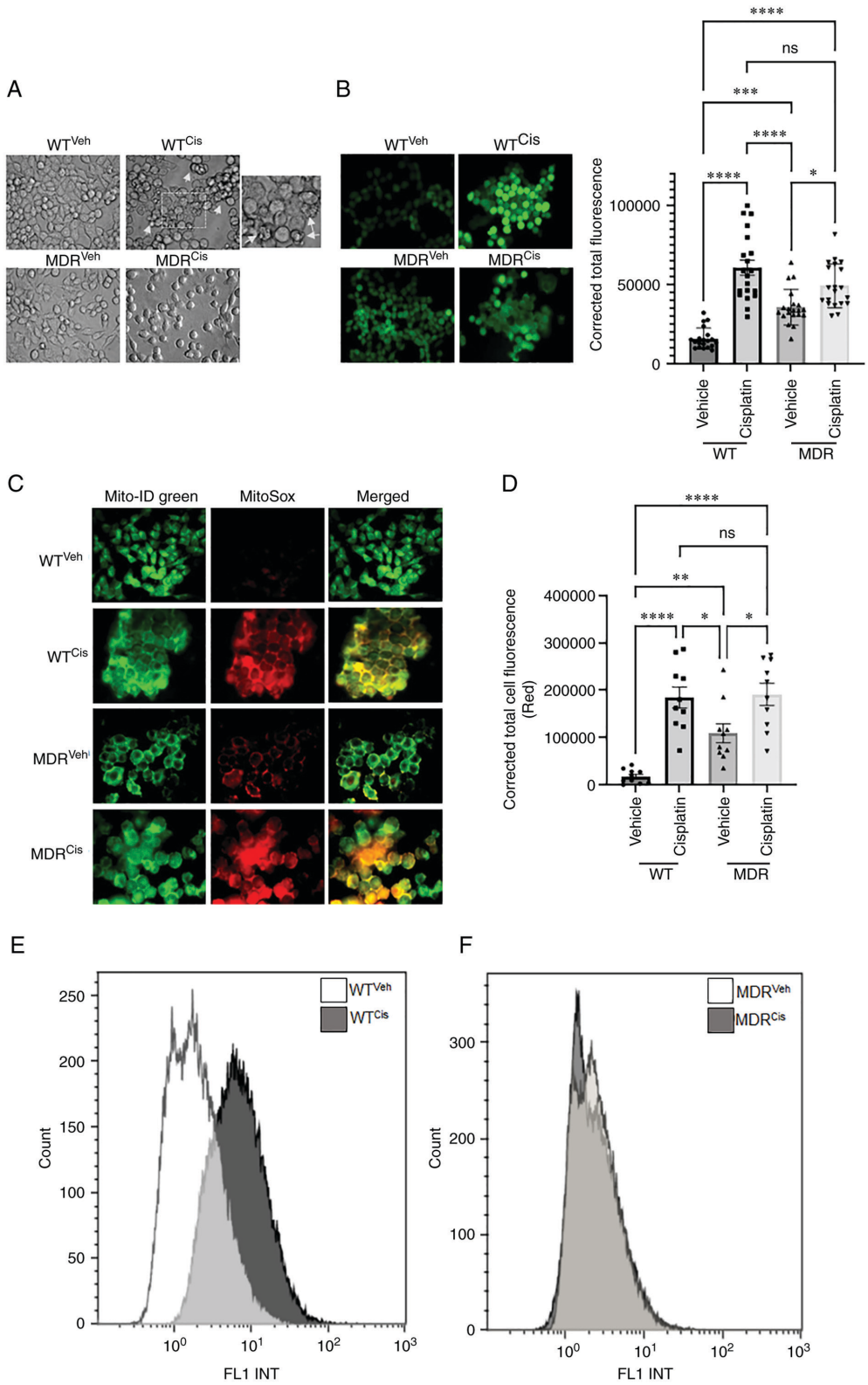

Figure S2. MDR HCT-116 cells are resistant to cisplatin-induced apoptosis. Representative flow cytometry data used for apoptosis analysis in vehicle and cisplatin-treated WT and MDR cells. These histograms are used for comparison between vehicle and cisplatin-treated WT and MDR cells presented in Fig. S1E and F. Quantification results of apoptosis analysis with vehicle and cisplatin treatment from these figures is presented in Fig. 1C. The values of '%Gated' used to plot Fig. 1C. Cis, cisplatin; FL1 INT, fluorescent light 1-integral time-off flight; FS INT, forward scatter-integral time-of-flight; MDR, multidrug resistant; SS INT, side scatter-integral time-of-flight; veh, vehicle; WT, wild-type.

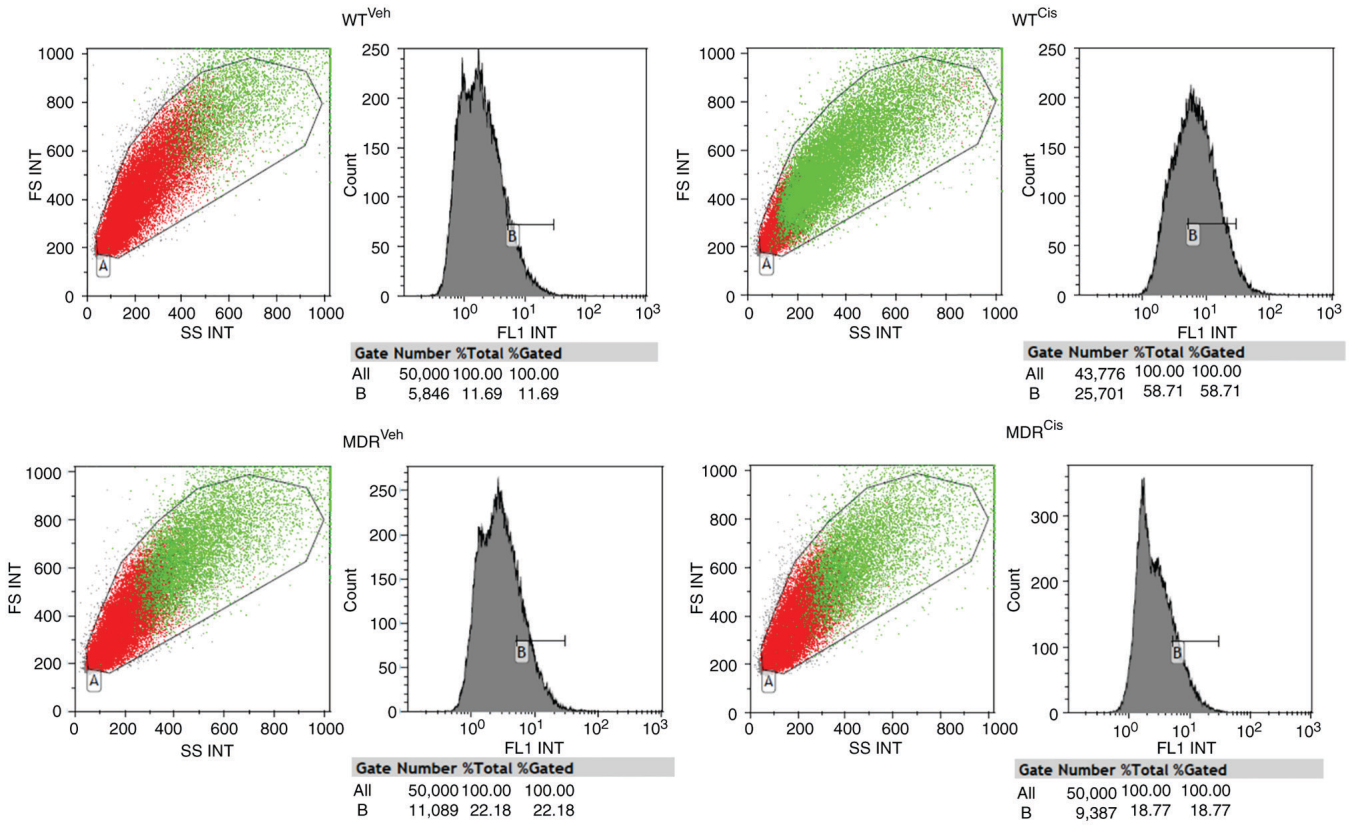

Figure S3. Cisplatin exposure induces apoptosis markers in WT HTC-116 cells compared with MDR cells. (A) Densitometric analysis of apoptosis markers from the western blotting images in Fig. 1E was conducted using ImageJ; one-way ANOVA was used for statistical analysis. (B) Densitometric analysis of AIF in the mitochondrial and nuclear protein extracts. (C) Nuclear/mitochondrial ratio of AIF. (D) c-Jun in nuclear protein expression from the western blotting images in Fig. 1F was conducted using ImageJ. One-way ANOVA was used for statistical analysis. *P<0.05; **P<0.01; ***P<0.001; ****P<0.0001. AIF, apoptosis-inducing factor; cis, cisplatin; MDR, multidrug resistant; ns, not significant; PARP, poly(ADP-ribose) polymerase 1; veh, vehicle; WT, wild-type.

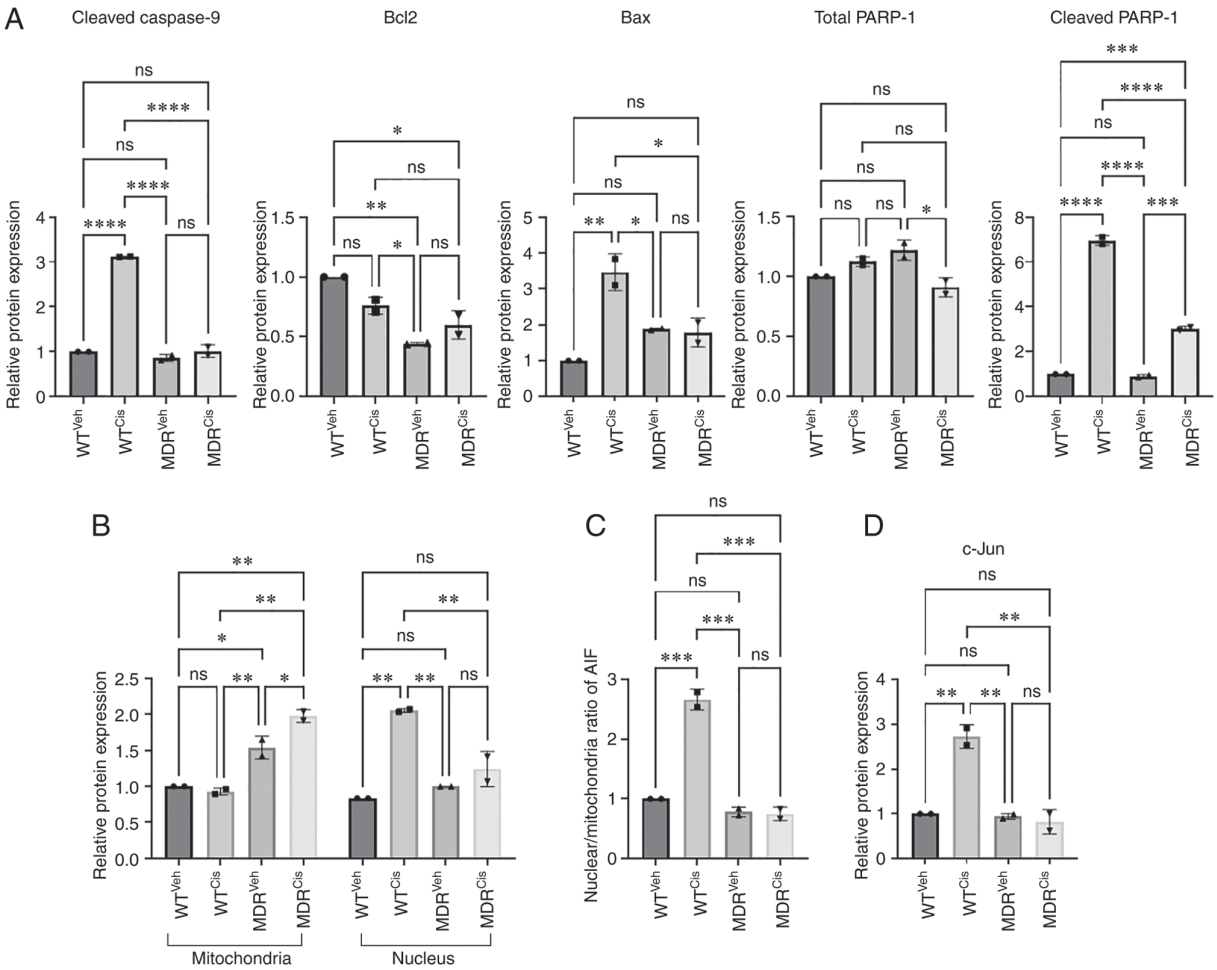

Figure S4. Cisplatin exposure induces AP1 DNA binding in WT HCT-116 cells. (A) Electrophoretic mobility shifts assay using non-radioactive consensus sequence of AP1 and (B) densitometric analysis using ImageJ software, showing higher DNA binding in WT^{Cis} cells compared with the WT^{Veh}. One-way ANOVA was used for statistical analysis. $^{*}P<0.05$; $^{**}P<0.01$. AP1, activator protein 1; cis, cisplatin; MDR, multi-drug resistant; ns, not significant; veh, vehicle; WT, wild-type.

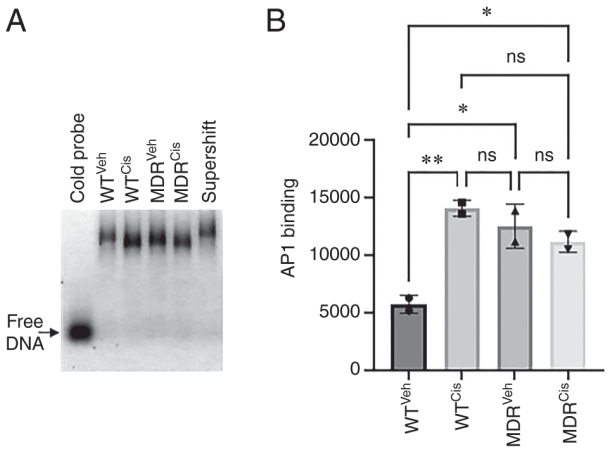

Figure S5. UPR is activated in MDR HCT-116 cells. (A) Densitometric analysis of UPR protein marker expression levels and (B) the ratio of phosphorylated/total protein expressions using ImageJ on the western blots presented in Fig. 2C. One-way ANOVA was used for statistical analyses. *P<0.05; **P<0.01; ***P<0.001. Cis, cisplatin; eIF2α, eukaryotic initiation factor 2α; GRP78, glucose-regulated protein 78; IRE1α, inositol-requiring kinase 1α; MDR, multidrug resistant; ns, not significant; p-, phosphorylated; PERK, PKR-like endoplasmic reticulum kinase; UPR, unfolded protein response; veh, vehicle; WT, wild-type.

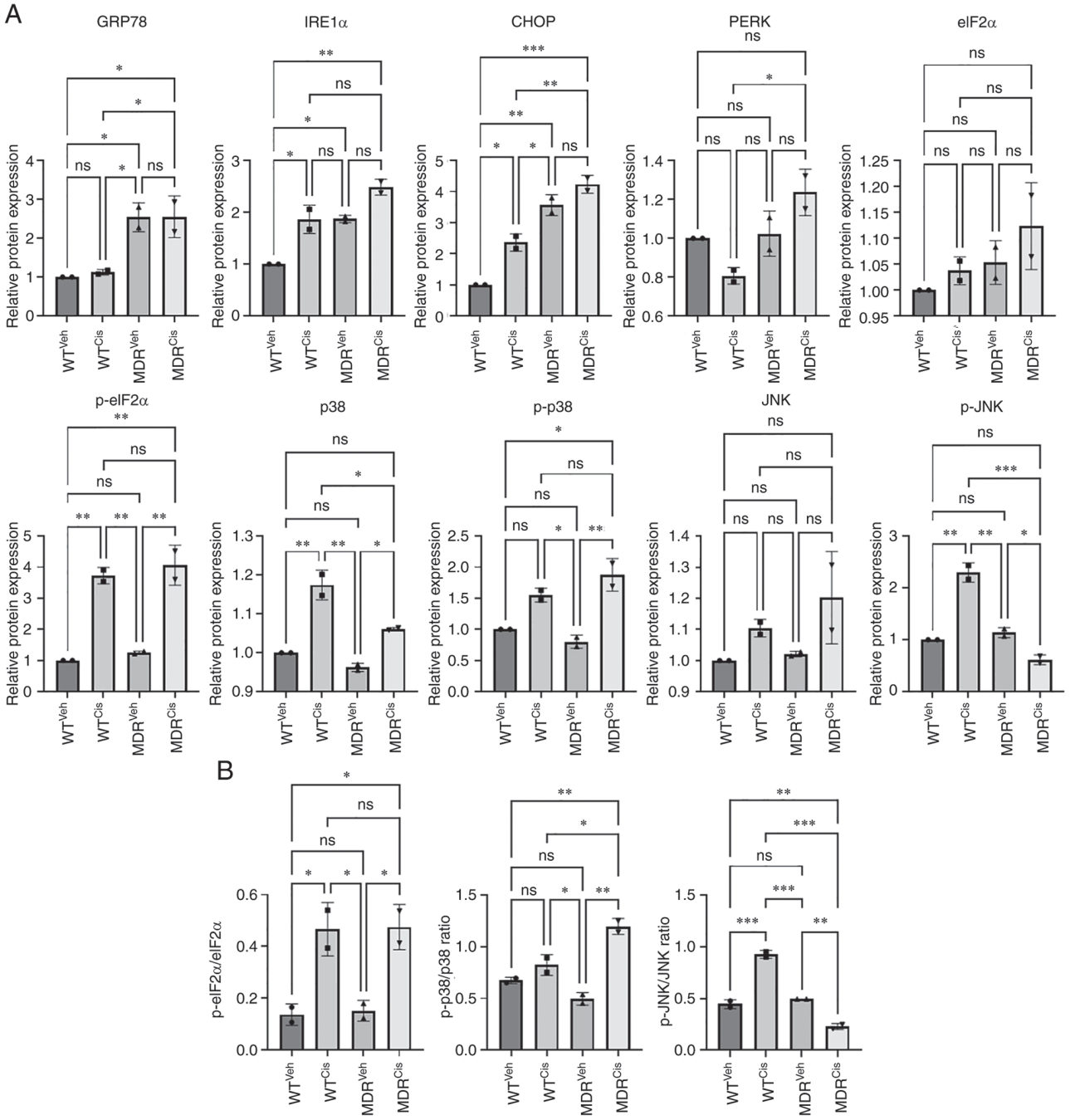

Figure S6. MDR HCT-116 cells show an unfolded protein response-mediated autophagy. WT and MDR HCT-116 cells were treated with 50 μM cisplatin or vehicle for 12 h. (A) Representative flow cytometry images and (B) quantification of cell autophagy analysis after staining with Cyto-ID® Autophagy reagent; one-way ANOVA was used for statistical analysis. (C) Densitometric analysis of the western blotting data (except LC3) presented in Fig. 2F was conducted using ImageJ; one-way ANOVA was used for statistical analyses. (D) Densitometric analysis of the ratio of LC3II/LC3I proteins presented in Fig. 2F; one-way ANOVA was used for statistical analysis. *P<0.05; **P<0.01; ***P<0.001; ****P<0.0001. ATG, autophagy-related gene; cas, caspase; FL1 INT, fluorescent light 1-integral time-of-flight; GSTO1, glutathione-S-transferase Ω-1; MDR, multidrug resistant; ns, not significant; WT, wild-type.

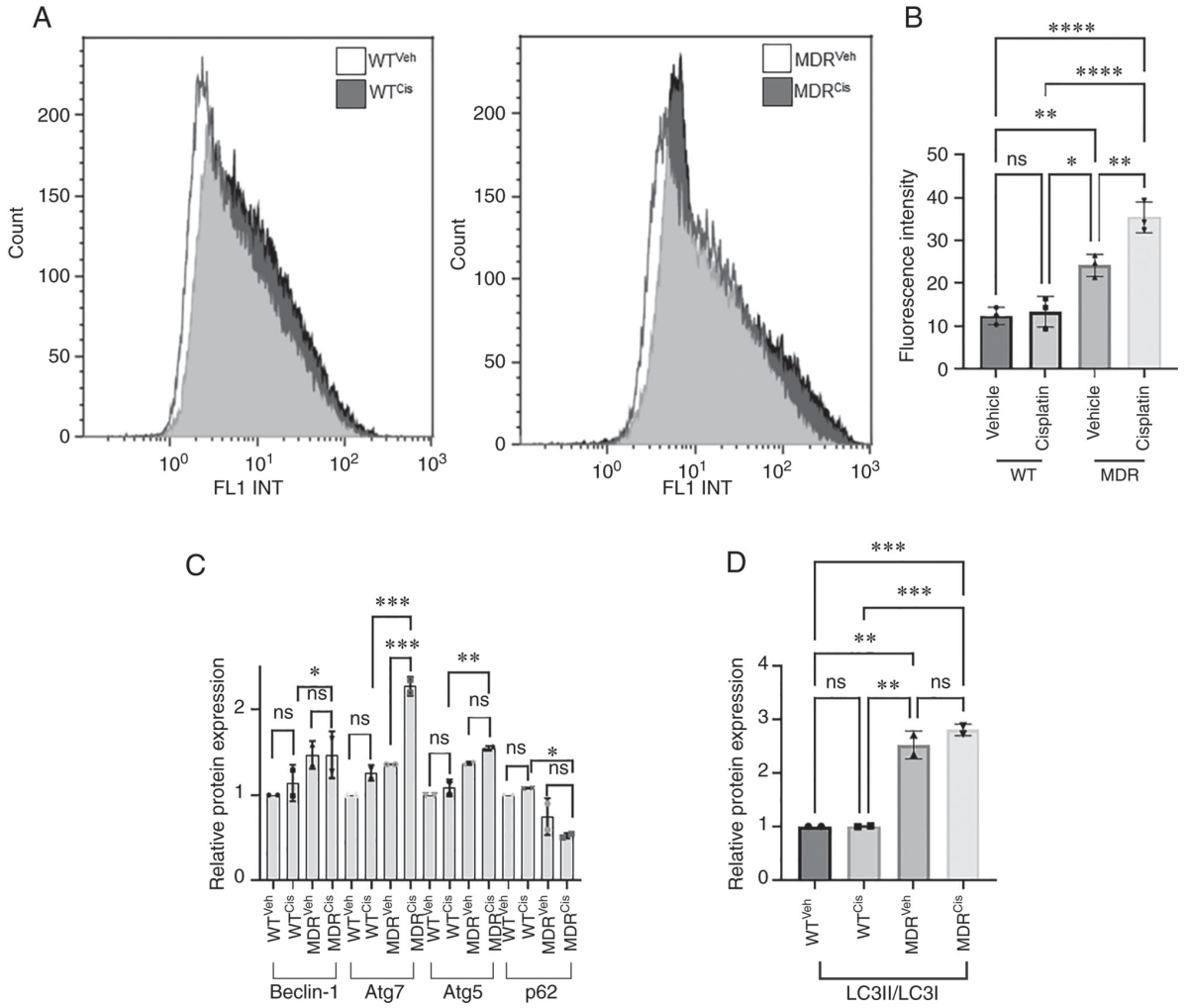

Figure S7. MDR HCT-116 cells exhibit an increase in autophagy. Representative flow cytometry data of autophagy analysis in vehicle and cisplatin-treated WT and MDR cells. These histograms are used for comparison between vehicle and cisplatin-treated WT and MDR cells presented in Fig. S6A, B. The values of '%Gated' used to plot Fig. S6B. Cis, cisplatin; FL1 INT, fluorescent light 1-integral time-of-flight; FS INT, forward scatter-integral time-of-flight; MDR, multidrug resistant; SS INT, side scatter-integral time-of-flight; veh, vehicle; WT, wild-type.

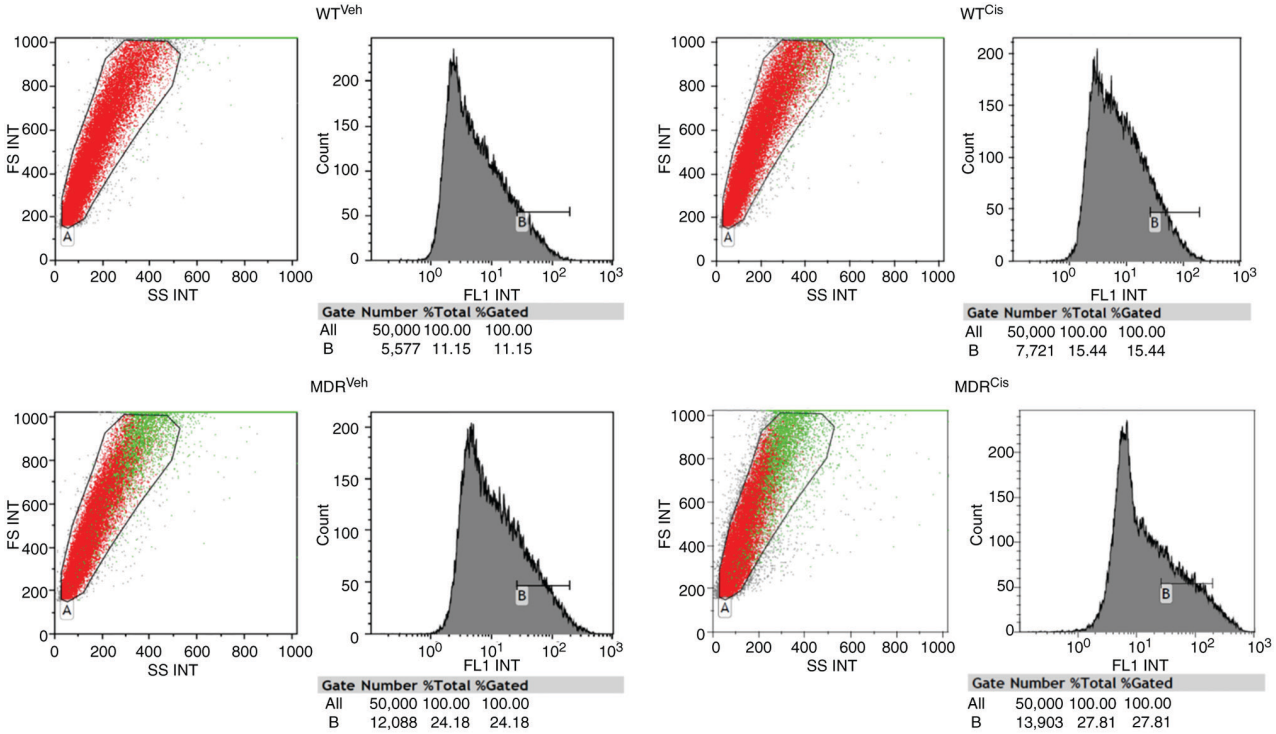

Figure S8. BAF-A1 treatment of MDR HCT-116 cells inhibited autophagy and sensitized the MDR cells to cisplatin. (A) Representative western blotting images of BAF-A1-treated, cisplatin-treated and co-treated MDR cells and densitometric analysis of autophagy markers (B) p62 and (C) LC3, and apoptosis markers (D) cleaved caspase 9, (E) cleaved caspase 3 and (F) cytochrome *c* using ImageJ. One-way ANOVA was used for statistical analyses. *P<0.05; **P<0.01; ***P<0.001. BAF-A1, bafilomycin-A1; cas, caspase; cyto *c*, cytochrome *c*; MDR, multidrug resistant; ns, not significant.

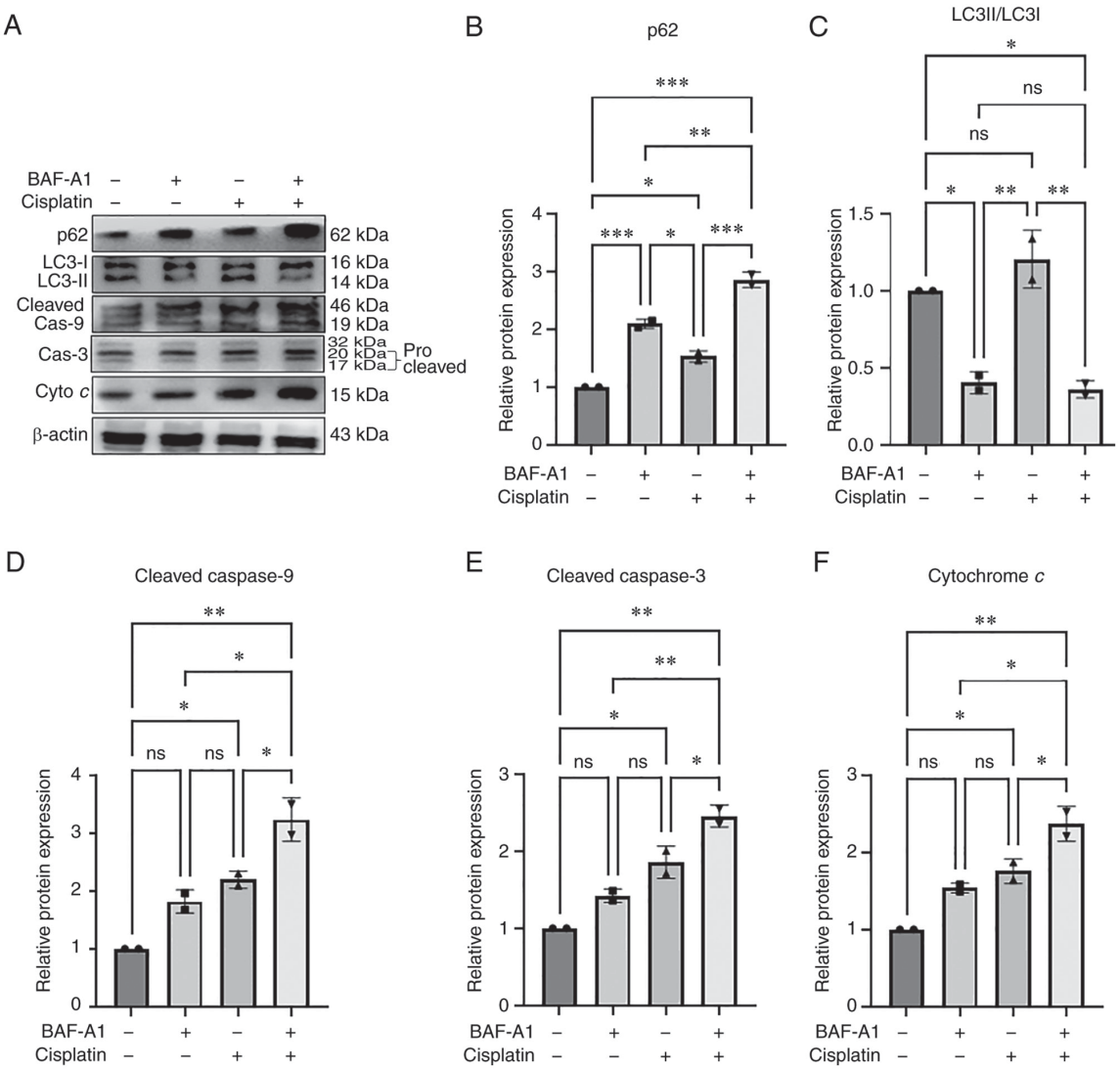

Figure S9. *GSTO1* activation in WT HCT-116 cells does not induce ER stress and UPR, whereas *GSTO1* knockdown in MDR cells reduces ER stress and UPR. (A) Representative western blotting images of ER stress- and UPR-related protein marker expression and (B) densitometric analysis using ImageJ in *GSTO1*-activated WT cells. A Mock vector was used as a control for both cases. (C) Representative flow cytometry image and (D) quantification of cell autophagy analysis after in the Mock and GSTO1-activated cisplatin-treated cells stained with Cyto-ID® Autophagy reagent. (E) Densitometric analysis of GSTO1 protein expression levels from the western blots in Fig. 3A and E was conducted using ImageJ; the data show the *GSTO1*-activation and -inhibition status in transfected WT and MDR cells, respectively. (F) Immunofluorescence detection of GFP expression in the Mock and *GSTO1*-KD plasmid transfected MDR cells (x100 magnification). (G) ER stress and UPR-related protein marker expression and (H) densitometry analysis using ImageJ in *GSTO1*-KD MDR cells. One-way ANOVA was used for statistical analyses. *P<0.05; **P<0.01. Act, activation; cis, cisplatin; ER, endoplasmic reticulum; FL1 INT, fluorescent light 1-integral time-of-flight; GRP78, glucose-regulated protein 78; GSTO1, glutathione-S-transferase Ω-1; IRE1α, inositol-requiring kinase 1α; KD, knockdown; MDR, multidrug resistant; ns, not significant; PERK, PKR-like endoplasmic reticulum kinase; UPR, unfolded protein response; veh, vehicle; WT, wild-type.

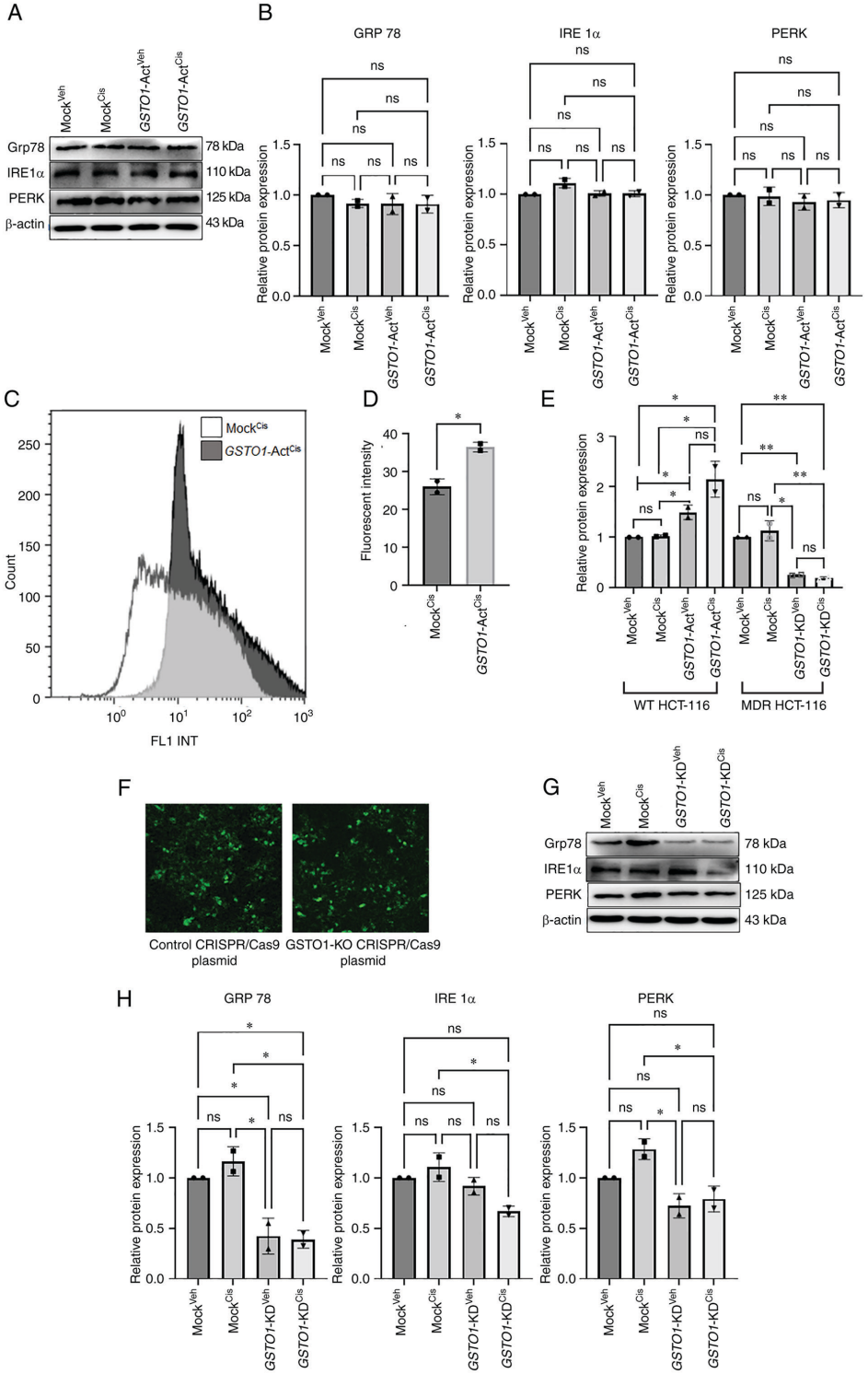

Figure S10. *GSTO1* activation in WT HCT-116 cells induces autophagy and *GSTO1* inhibition in MDR cells inhibits autophagy. (A) Densitometric analysis of autophagy- and apoptosis-related marker protein expression levels in veh- or cis-treated WT cells, from the western blots presented in Fig. 3A, was conducted using ImageJ. (B) Densitometric analysis of autophagy- and apoptosis-related marker protein expression levels in veh- or cis-treated MDR cells, from the western blots presented in Fig. 3E, was conducted using ImageJ. One-way ANOVA was used for statistical analyses. *P<0.05; **P<0.01; ***P<0.001; ****P<0.0001. Act, activation; cis, cisplatin; GSTO1, glutathione-S-transferase Ω-1; KD, knockdown; MDR, multidrug resistant; ns, not significant; veh, vehicle; WT, wild-type.

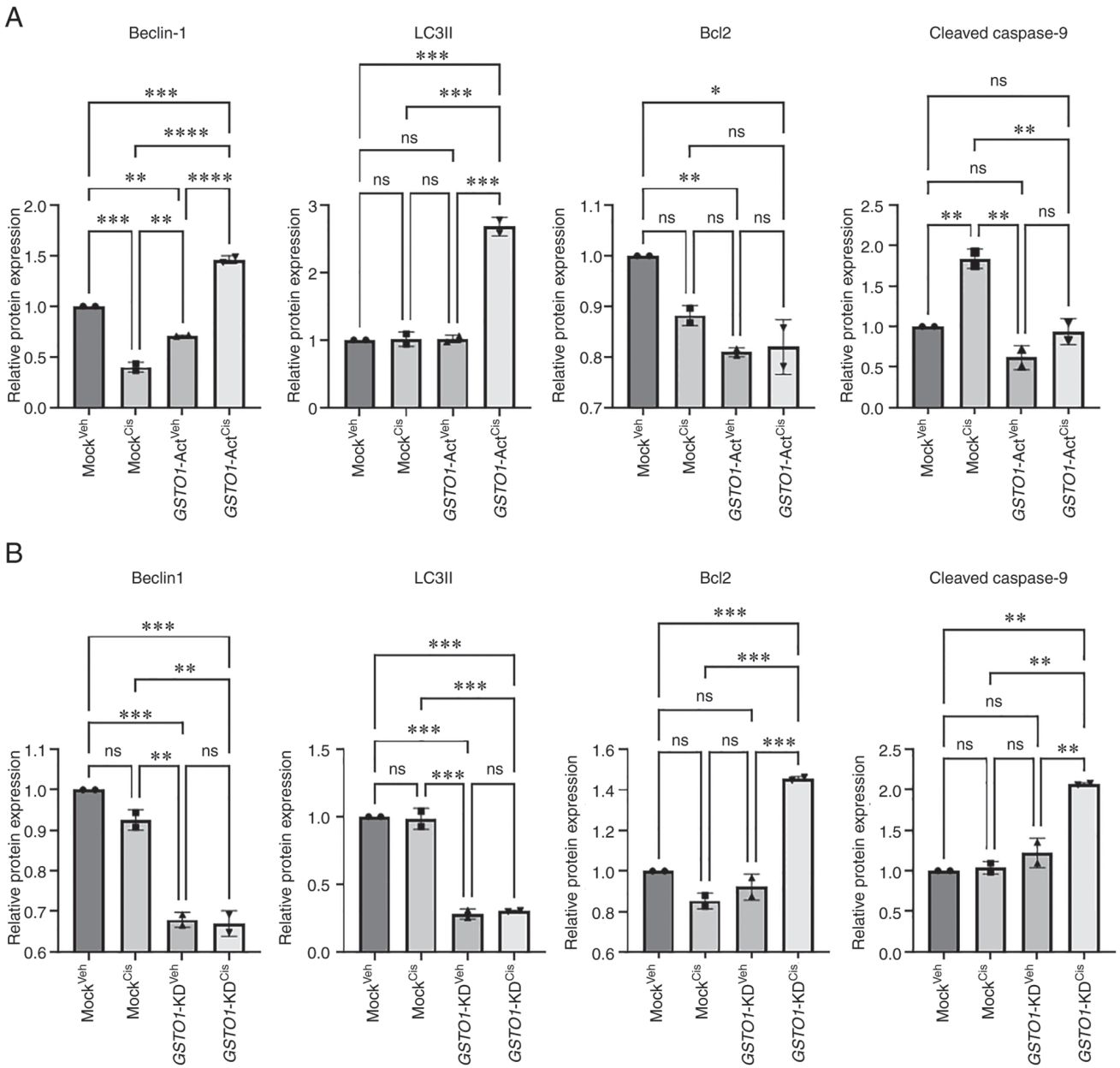

Figure S11. *GSTO1* activation in WT HCT-116 cells induces autophagy. Representative flow cytometry data of autophagy analysis in the cisplatin-treated Mock and *GSTO1*-Act cells. These histograms are used for comparisons presented in Fig. S9C. Quantification results of autophagy analysis from these figures is presented in Fig. S9D. The values of '%Gated' used to plot Fig. S9D. Act, activation; cis, cisplatin; FL1 INT, fluorescent light 1-integral time-of-Flight; FS INT, forward scatter-integral time-of-flight; GSTO1, glutathione-S-transferase Ω-1; SS INT, side scatter-integral time-of-flight.

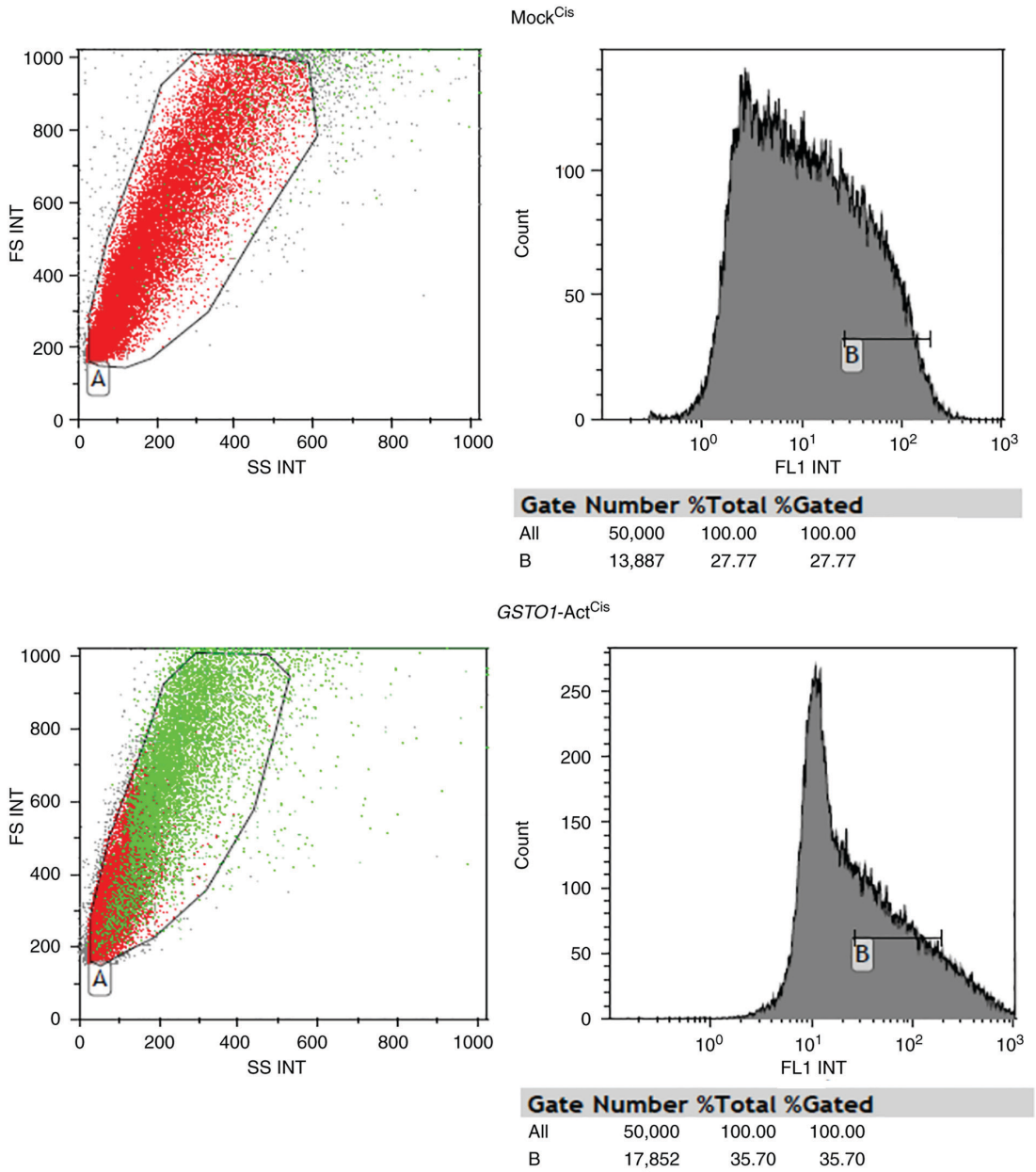

Figure S12. Inhibition of GSTO1-TNFαIP3/A20 interaction sensitizes MDR cells to cisplatin. Densitometric analysis of GSTO1 and TNFαIP3/A20 protein expression levels, as well as apoptosis- and autophagy-related markers using ImageJ in *GSTO1*, *TNFαIP3/A20* single-KD and double-KD MDR cells from the western blotting data presented in Fig. 5G. One-way ANOVA was used for statistical analyses. *P<0.05; **P<0.01; ***P<0.001; ****P<0.0001. Cis, cisplatin; GSTO1, glutathione-S-transferase Ω-1; TNFαIP3/A20, TNF-α-induced protein 3/zinc-finger protein A20; ns, not significant; KD, knockdown.

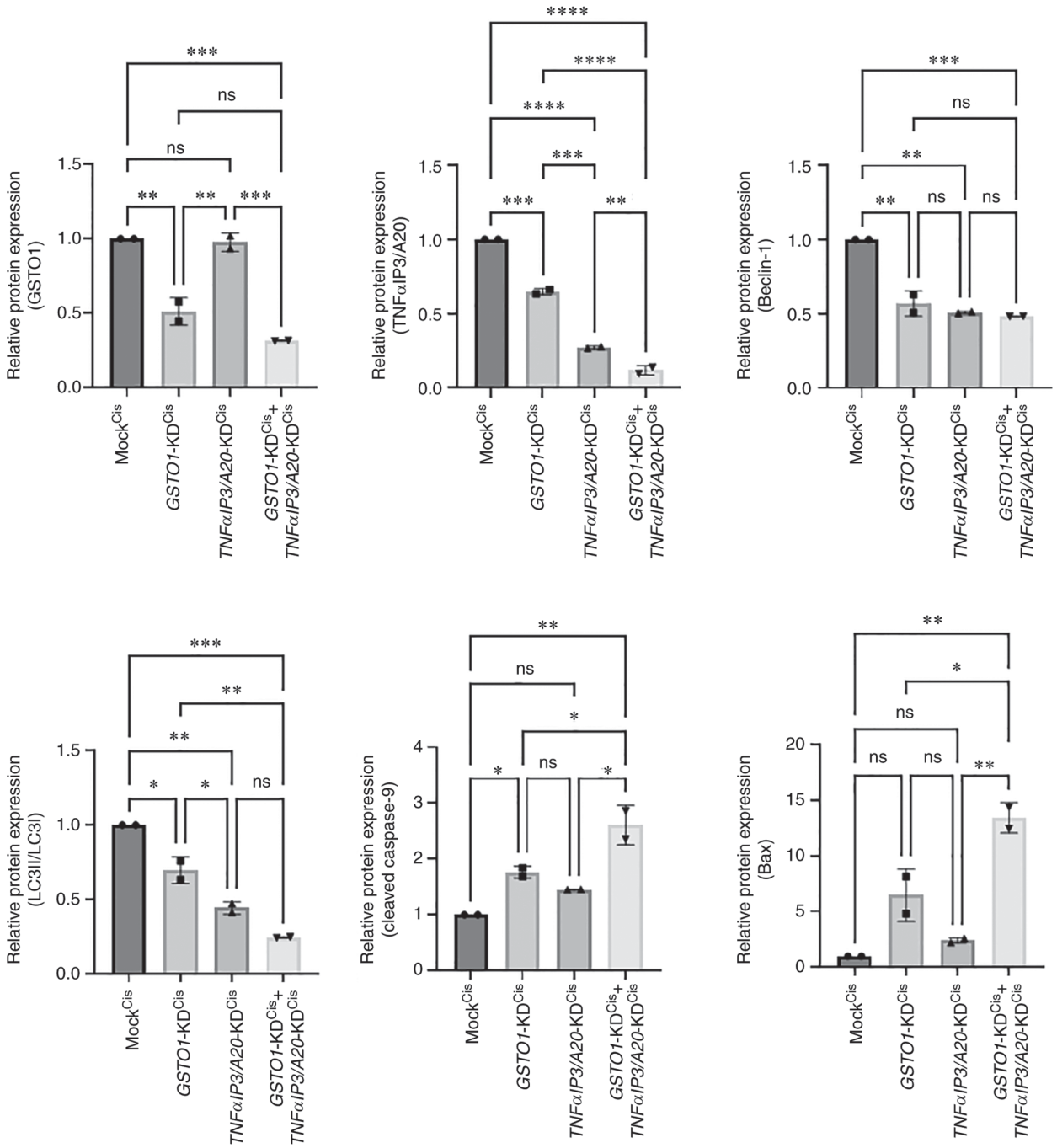

Figure S13. Schematic diagram of the mechanism of GSTO1-mediated drug resistance in colon cancer cells. GSTO1-TNFαIP3/A20 interaction is important to develop multi-drug resistance in HCT-116 cells. GSTO1 activation results autophagy cell survival in WT cells, whereas GSTO1 inhibition in MDR cells activates apoptotic cell death. GSTO1, glutathione-S-transferase Ω-1; MDR, multidrug resistant; TNFαIP3/A20, TNF-α-induced protein 3/zinc-finger protein A20; WT, wild-type.